JM6/ANDREWS

CR-128647

NTIS: HC $3.00

E-2708

ENERGY MANAGEMENT DURING THE SPACE SHUTTLE TRANSITION

by

Robert F. Stengel

August 1972

CHARLES STARK DRAPER LABORATORY

MASSACHUSETTS INSTITUTE OF TECHNOLOGY

CAMBRIDGE, MASSACHUSETTS, 02139

E-2708

ENERGY MANAGEMENT DURING THE SPACE SHUTTLE TRANSITION

by

Robert F. Stengel

Charles Stark Draper Laboratory
Massachusetts Institute of Technology
Cambridge, Massachusetts
02139

Approved: David C Fraser Date: 28 August 1972

D. C. FRASER, DIRECTOR, CONTROL AND FLIGHT DYNAMICS
APOLLO GUIDANCE AND NAVIGATION PROGRAM

Approved: D. G. Hoag for Date: 30 Aug 72

R. H. BATTIN, DIRECTOR, MISSION DEVELOPMENT
APOLLO GUIDANCE AND NAVIGATION PROGRAM

Approved: David G Hoag Date: 30 Aug 72

D. G. HOAG, DIRECTOR
APOLLO GUIDANCE AND NAVIGATION PROGRAM

Approved: Ralph R. Ragan Date: 30 Aug 72

R. R. RAGAN, DEPUTY DIRECTOR
CHARLES STARK DRAPER LABORATORY

ACKNOWLEDGEMENT

This report was prepared under DSR Project 55-40800, sponsored by the Manned Spacecraft Center of the National Aeronautics and Space Administration through Contract NAS 9-10268.

ENERGY MANAGEMENT DURING THE SPACE SHUTTLE TRANSITION

Robert F. Stengel
Charles Stark Draper Laboratory
Massachusetts Institute of Technology
Cambridge, Massachusetts

ABSTRACT

An approach to calculating optimal, gliding flight paths of the type associated with the space shuttle's transition from entry to cruising flight is presented. Kinetic energy and total energy (per unit weight) replace velocity and time in the dynamic equations, reducing the dimension and complexity of the problem. The capability for treating integral and terminal penalties (as well as Mach number effects) is retained in the numerical optimization; hence, stability and control boundaries can be observed as trajectories to the desired final energy, flight path angle, and range are determined. Numerical results show that the "jump" to the "front-side of the L/D curve" need not be made until the end of the transition and that the dynamic model provides a conservative range estimate. Alternatives for real-time trajectory control are discussed.

INTRODUCTION

The space shuttle orbiter's return from orbit is marked by three mission phases whose flight dynamics and constraints are fundamentally different. (Fig. 1.) The entry phase occurs at angles of attack (α) greater than that required for maximum lift-drag ratio, L/D, (the "backside of the L/D curve") in order to meet heating constraints. This phase passes through a region of radio frequency "blackout" during which time ground-based navigational aids cannot be used; it terminates at mesospheric altitude and supersonic velocity. Large range and cross-range maneuvers can be made during the entry phase. The entry phase is matched to the terminal area and landing phase by a transition phase, which further decelerates the vehicle to subsonic velocity as altitude decreases to approximately 40,000 ft. Angle of attack shifts from the backside to the frontside of the L/D curve during transition, the principal constraints being stability and control boundaries.[1] Ranging control can be continued during this phase, although it could be necessary to limit or suspend ranging in flight regions where attitude control is particularly difficult. The shuttle's terminal area and landing phase will be similar to that of standard aircraft operations, with the exception that provisions must be made for unpowered flight.

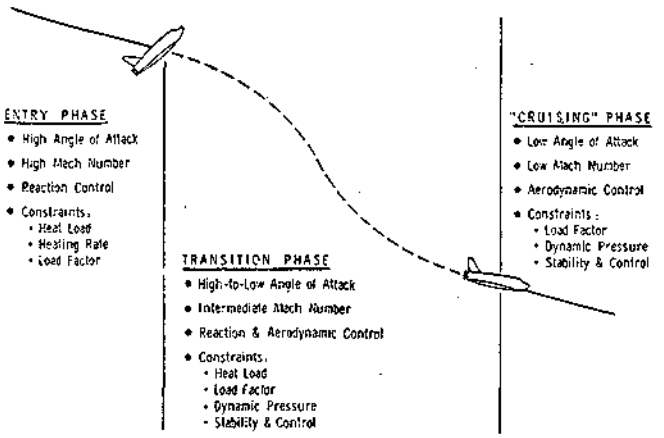

Figure 1. Flight phases during the return from orbit.

Trajectory and guidance computations for the transition phase are complicated by the rapidly changing flight environment and by the interdependence of state and control. Mach number, angle-of-attack, and air-density effects are strong, and their ranges of values on any given transition trajectory are large. Whether it is used as an in-line part of an explicit guidance law or as a source of a priori nominal profiles for a simplified guidance scheme, a fast, reliable means of generating transition flight paths and control histories which meet engineering and navigational requirements will be useful.

A numerical approach to defining optimal gliding trajectories is presented in this paper. The optimization problem is made easier by simplifying the model of flight dynamics and by substitution of variables. This allows the number of state and adjoint variables to be integrated to be reduced. Velocity is replaced by kinetic energy, and total energy takes the place of time as the independent variable. The requirement for descending to a particular altitude with a given velocity allows the open end-time of the original problem to be replaced

by fixed terminal energy, eliminating the additional complexity of end-point adjustment. A steepest-descent algorithm with near-optimal step-sizing rapidly minimizes a cost function consisting of integral and terminal penalties. The integral penalties provide phugoid damping (minimizing dynamic pressure- and load factor peaks) and assure that α remains within stability and control boundaries. The terminal penalties (which are soft constraints) force the final state into the desired region. As is to be expected with any iterative solution of equations, the speed of convergence is greatly affected by the choice of initial control profile; however, it appears that a small family of starting control histories will initiate convergence to an acceptable flight path within a few iterations (i.e., less than half a dozen).

DEVELOPMENT OF EQUATIONS

Transformation of Variables

The equations of motion for the two-dimensional trajectories considered here make use of the flat-earth approximations, on the basis that glide range and altitude changes during the transition maneuver are small compared to the earth's radius and that velocity is decidedly sub-orbital. With the further assumption of an air-density profile, $\rho(H)$, which is exponential with altitude, the equations for velocity magnitude (V), flight path angle (γ), altitude (H), and range (R) are

$$\dot{V} = -C_D\, k e^{-\beta H} V^2/2 - g \sin\gamma \qquad (1$$

$$\dot{\gamma} = C_L\, k e^{-\beta H} V/2 - (g/V)\cos\gamma \qquad (2$$

$$\dot{H} = V \sin\gamma \qquad (3$$

$$\dot{R} = V \cos\gamma \qquad (4$$

where β is the inverse scale height of the atmosphere, g is the average gravitational constant in the transition altitude interval, and the constant, k, combines reference area (S), vehicle mass (m), and reference air density (ρ_o) as

$$k = \frac{S\rho_o}{m} \qquad (5$$

Angle of attack (α), is taken as the control variable; it enters the equations through the lift- and drag coefficients (C_L and C_D), which are also arbitrary functions of Mach number (M).

The kinetic energy per unit weight is

$$K = V^2/2g, \qquad (6$$

and it is seen that K can replace V in Eq. (1) to (4). Differentiating Eq. (6) with respect to time,

$$\dot{K} = V\dot{V}/g \qquad (7$$

and the revised set of equations is

$$\dot{K} = -C_D\, k e^{-\beta H}(2gK^3)^{1/2} - (2gK)^{1/2}\sin\gamma \qquad (8$$

$$\dot{\gamma} = C_L\, k e^{-\beta H}(gK/2)^{1/2} - (g/2K)^{1/2}\cos\gamma \qquad (9$$

$$\dot{H} = (2gK)^{1/2}\sin\gamma \qquad (10$$

$$\dot{R} = (2gK)^{1/2}\cos\gamma \qquad (11$$

Equations (8) to (11) have no explicit dependence on time; therefore, time can be replaced as the independent variable, and the number of equations can be reduced by one. Recent papers have replaced time by altitude[2] and flight path angle[3] to good effect. There is a potential difficulty in choosing K, γ, or H to be the independent variable, as there is no assurance that these quantities will decrease monotonically with time. In particular, a phugoid oscillation in near-horizontal flight causes the time-rate-of-change of all these variables to change sign. As a consequence, it becomes necessary to transit singular points, and the control profile becomes multi-valued. There is a combination of K and H which is guaranteed to be monotonic in gliding flight (although not in powered flight[4]). It is, of course, the total energy per unit weight, or specific total energy,

$$E = K + H, \qquad (12$$

which is always dissipated by the effect of aerodynamic drag. This is easily seen, because

$$\dot{E} = \dot{K} + \dot{H}, \qquad (13a$$

and Eq. (8) and (10) show that

$$\dot{E} = -C_D\, k e^{-\beta H}(2gK^3)^{1/2} \qquad (13b$$

Equation (13b) is always less than zero. The derivative

$$d(\,)/dE = [d(\,)/dt]/[dE/dt] \equiv (\,)' \qquad (14$$

is thus well-behaved everywhere on the gliding path, and the differential equation for either K or H can be eliminated using Eq. (12) and (14). Choosing H to be eliminated, the differential equations of motion using specific total energy (E) as the independent variable become

$$K' = 1 + \sin\gamma/C_D\mu \qquad (15$$

$$\gamma' = (-C_L + \cos\gamma/\mu)/2C_D K \qquad (16$$

$$R' = -\cos\gamma/C_D\mu \qquad (17$$

where

$$\mu = k e^{-\beta H_K} \qquad (18$$

and H is determined from Eq. (12). μ can also be written as qS/W, i.e., the dynamic pressure (q) divided by wing loading (W/S).

Expressing the vehicle dynamics in terms of total energy has several advantages in addition to eliminating a differential equation. The time to execute the transition maneuver is inconsequential; given a set of initial conditions on V, γ, H, and R, the maneuver must be defined to match final conditions on the same variables, subject to constraints which are functions of the state and control. V and H are combined in E; hence, the running interval $[E_o, E_f]$ is fixed and well-defined. Control histories and gains are then computed as functions of energy rather than time-to-go. This introduces a feedback relationship between the vehicle's state and control, and it eliminates the problem of running out of gains and nominal control profile if time-to-go is exceeded before the terminal flight condition is reached (for information, time-to-go can be calculated using Eq. (13b), since $dt = dE/\dot{E}$). A final advantage is that the partial derivatives necessary to describe perturbations about a given trajectory are simpler and fewer in number (see following sections).

Equations (6), (12) and (15-17) correspond exactly to Eq. (1-4); further simplifications can be made for transition trajectories. It is observed that flight path angle rates are negligible, i.e., that load factor is close to 1 during the transition.[1] Assuming that $\dot{\gamma} = 0$ leads to $\gamma' = 0$. The algebraic solution to Eq. (16) is then

$$\cos\gamma = C_L\mu \tag{19}$$

and the number of equations to be integrated is reduced to 2. Alternatively, the flight path angle can be assumed small during the transition,[1] leading to a third-order system with $\cos\gamma \cong 1$ and $\sin\gamma \cong \gamma$. Both simplifications are examined further, and the optimization continues with the latter approximation.

Second- and Third-Order Dynamic Models

With negligible γ rates, Eq. (19) applies, and the dynamical equations (for $\gamma \lesssim 0$) are

$$K' = 1 \mp (1 - C_L^2\mu^2)^{1/2} / C_D\mu \tag{20}$$

$$R' = -C_L/C_D \tag{21}$$

The simplicity of the range equation provides a well-known result for gliding flight, namely that glide range between two energy-states is maximized by flying at L/D_{max}. This is easily seen, since

$$R = \int_{E_o}^{E_f} (-C_L/C_D)\, dE \quad , \quad E_o > E_f \tag{22}$$

The integral is maximized when the integrand is minimized, which occurs at L/D_{max}. This result depends not on small γ but on negligible $\dot{\gamma}$, and it allows C_L and C_D to be functions of M as well as α.

In order to study optimal paths, it is necessary to find the sensitivity of the state equations to small variations in K, R, and α. Neglecting C_{L_M} and C_{D_M}, the three non-zero partial derivatives are

$$\frac{\partial K'}{\partial \alpha} = \pm \frac{1}{(C_D^2\mu)} \left[\frac{\mu C_D C_L C_{L_\alpha} - (1 - C_L^2\mu^2) C_{D_\alpha}}{(1 - C_L^2\mu^2)^{1/2}} \right] \tag{23}$$

$$\frac{\partial R'}{\partial \alpha} = -\left(\frac{C_D C_{L_\alpha} - C_L C_{D_\alpha}}{C_D^2} \right) \tag{24}$$

$$\frac{\partial K'}{\partial K} = \pm \frac{\mu_K}{C_D} \left[\frac{1 - C_L^2(1 - \mu^2)}{(1 - C_L^2\mu^2)^{1/2}} \right] \tag{25}$$

where

$$\mu_K = \mu (\beta + 1/K) \tag{26}$$

These derivatives are well-posed for small perturbations about gliding flight paths, with one exception: the denominator of Eq. (23) and Eq. (25) can lead to difficulty. The denominator is actually $\sin\gamma$; hence the partials of K' become infinite in horizontal flight. When $C_L\mu > 1$, Eq. (19) is no longer valid, and the denominator becomes the square root of a negative number. It is likely that both difficulties will be encountered in a numerical optimization – if not on the optimal path, on a previous iteration. For these reasons, the second-order model will not be pursued; however, it is interesting to note that for planar, gliding trajectories without integral or terminal-range penalties, the equations required for optimization (see next section) are scalar. With a terminal-range penalty, the range adjoint variable is non-zero but constant, leaving a single differential equation to be solved for the kinetic energy adjoint variable and a two-component control correction. The conventional assumption of a "parabolic drag polar" (C_L linear in α, C_D quadratic in C_L) simplifies Eq. (20-25) further, although the assumption is valid only for subsonic flight.

In the second approximation, the rate-of-change of flight path angle is not limited, but γ is assumed small. Equations (15-17) can be expressed as the vector equation

$$\underline{x}' = \underline{f}(\underline{x}, \alpha) \tag{27}$$

where $x_1 = K$, $x_2 = \gamma$, $x_3 = R$, and

$$f_1 = 1 + x_2/C_D\mu \tag{28}$$

$$f_2 = (-C_L + 1/\mu)/2C_D x_1 \tag{29}$$

$$f_3 = -1/C_D\mu \tag{30}$$

Equation (30) shows that $C_D\mu$, the drag deceleration, must be minimized to maximize range. Again assuming that C_{L_M} and C_{D_M} are negligible, 7 of the 12 partial derivatives with respect to x and α are non-zero. They are

$$f_{1_{x_1}} = -x_2(\beta + 1/x_1)/C_D\mu \quad (31$$

$$f_{1_{x_2}} = 1/C_D\mu \quad (32$$

$$f_{2_{x_1}} = [\,C_L - (2 + \beta x_1)/\mu\,]\,/2C_D x_1^2 \quad (33$$

$$f_{3_{x_1}} = (\beta + 1/x_1)/C_D\mu \quad (34$$

$$f_{1_\alpha} = -x_2 C_{D_\alpha}/C_D^2\mu \quad (35$$

$$f_{2_\alpha} = [\,-C_{L_\alpha} + C_{D_\alpha}(C_L - 1/\mu)/C_D\,]\,/2C_D x_1 \quad (36$$

$$f_{3_\alpha} = C_{D_\alpha}/C_D^2\mu \quad (37$$

The principal virtues of the small-angle approximation are computational, in that the number of partial derivatives is reduced, and there are no trigonometric functions or square roots to be evaluated. These attributes, plus the coincidence of similar terms in Eq. (28-37), make the third-order model hardly more complex than the second-order model. With range open, the state dimension is two. A terminal-range penalty increases the state dimension to 3, but the range adjoint variable is again constant, leaving two adjoint variables to be evaluated by numerical integration.

Optimization Using the Third-Order Model

It is desired to minimize a cost function consisting of terminal and integral penalties, subject to the dynamic constraint of Eq. (27). The augmented cost function, J, for fixed end condition is

$$J = (\underline{x}_f - \underline{x}_D)^T \underline{\underline{Q}} (\underline{x}_f - \underline{x}_D) + \int_{E_o}^{E_f} \{\mathscr{L}(\underline{x}, \alpha) + \underline{\lambda}^T[\,\underline{f}(\underline{x}, \alpha) - \underline{x}'\,]\}\, dE, \; E_o > E_f \quad (38$$

where $\underline{\underline{Q}}$ is a constant, diagonal matrix weighting the squared-error between achieved- and desired final state, $\mathscr{L}$ is a penalty function whose integral must be minimized, and $\underline{\lambda}$ is the vector adjoint of $\underline{x}$. The state vector is a function of E through Eq. (27), while $\underline{\lambda}(E)$ is found from

$$\underline{\lambda}'(E) = -\underline{f}_x^T(E)\,\underline{\lambda}(E) - \underline{\mathscr{L}}_x^T(E) \quad (39$$

with

$$\underline{\lambda}(E_f) = 2\underline{\underline{Q}}(\underline{x}_f - \underline{x}_D) \quad (40$$

Having obtained a trajectory from Eq. (27) with an initial control profile, $\alpha(E)$, the angle-of-attack history is improved on succeeding iterations by the perturbation

$$\delta\alpha(E) = -\epsilon(\mathscr{L}_\alpha + \underline{\lambda}^T \underline{f}_\alpha)^T \quad (41$$

where ϵ is a near-optimal step-size obtained by a one-dimensional search of $J(\epsilon)$. A quadratic approximation, $\tilde{J}(\epsilon)$, is found by evaluating the costs of three trajectories with control profiles $\alpha_o(E)$, $\alpha_o(E) + \epsilon_o\delta\alpha(E)$, and $\alpha_o(E) + 2\epsilon_o\delta\alpha(E)$. The iteration is completed by choosing the ϵ which minimizes the variation of $\tilde{J}$ with respect to ϵ. Additional test trajectories are computed if it is apparent that a significant improvement can be made, e.g., if

$$\epsilon(\min \tilde{J}) > 2\epsilon_o.$$

Although terminal-range corrections are most readily made by varying α during the early portion of the trajectory, it is found that no combination of penalty weights provides this obvious control correction. Equation (41) tends to reach its largest values in the latter portion of the flight. A simple artifice which retains the essential ingredients of the steepest-descent algorithm overcomes the problem. On the first one or two iterations (depending on terminal-range error), the step-size, ϵ_o, is multiplied by a ramp function, which equals 1 at E_o and 0 at E_f; hence, the corrections are attenuated as the terminal point is approached. The ramp weighting allows large changes in range with little change in terminal V and γ, which are primarily determined by the control profile in the latter portion of the flight.

The integral penalty function ($\mathscr{L}$) contains terms which enforce control boundaries and which introduce trajectory damping. Angle-of-attack boundaries imposed by elevator "control power" and embedded regions of instability which are functions of Mach number have been considered previously.[1] In the present paper, the α-penalty is simply

$$\mathscr{L}_1 = \begin{cases} c_1(\alpha - \alpha_1)^2 & , \quad \alpha < \alpha_1 \\ 0 & , \quad \alpha_1 \le \alpha \le \alpha_2 \\ c_2(\alpha - \alpha_2)^2 & , \quad \alpha > \alpha_2 \end{cases} \quad (42$$

with α_1 and α_2 chosen as 3° and 50° respectively (c_1 and c_2 must be negative for the energy integral of $\mathscr{L}$ to be positive). The upper limit roughly corresponds to the highest hypersonic trim angle-of-attack likely to be obtained for a delta-wing space shuttle with negative-maximum elevon deflection. The trim limit is sensitive to center-of-gravity location and could be sharply reduced by aft movement of the c.g.; it also decreases with decreasing M. The 3°-limit is arbitrarily chosen to maintain positive load factor. $\mathscr{L}_1$ is academic for the numerical results which follow. It comes into play during numerical iteration, but none of the optimal profiles presented here follow a control boundary.

Phugoid oscillation, which results from a lightly damped interchange of kinetic- and potential energy,[5] leads to load factor and dynamic pressure

overshoots, as well as γ and pitch attitude (θ) oscillation. The oscillation is forced by the continually changing flight condition; it can be reduced only by a varying α (which may occur somewhat automatically in planar cases by redefining the control variable to be $\theta = \gamma - \alpha$, as in Ref. 6). Penalties on load factor, $\dot{\gamma}$, or dynamic pressure can be employed to reduce the phugoid oscillation.

Load factor and $\dot{\gamma}$ penalties are closely related. The load factor is a function of both C_L and C_D, while (from Eq. (2)), $\dot{\gamma}$ is a function only of C_L. Analogously, a penalty on γ'^2 using Eq. (29) can be formed. The penalty has been used with some success, principally because it is a function of both the state and the control.

Dynamic pressure (q) is less successful in providing trajectory damping, because it is an implicit function of the control. The dynamic pressure can be expressed as

$$q = \frac{1}{2} \rho V^2$$

$$= \rho g x_1 , \tag{43}$$

and it is clear that q is an explicit function of the state only. Similar difficulties with state constraints can be solved by differentiating the constraint with respect to the independent variable until the control appears.[7] For dynamic pressure, a single differentiation is sufficient, as

$$q' = q (\rho x_1' + \rho' x_1)$$

$$= q [(\beta x_1 + 1) f_1 - \beta x_1] \tag{44}$$

and f_1 is a function of α through C_D (Eq. (28)). Equation (44) shows that the q' penalty is primarily a kinetic energy rate (x_1') penalty which is weighted by air density. The γ' penalty damps angular orientation of the velocity vector, while the q' penalty provides kinetic energy damping. The latter has been found to be more effective, and the trajectory damping penalty function used here is

$$\mathcal{L}_2 = c_3 q'^2, \qquad c_3 < 0, \tag{45}$$

with the partial derivatives

$$\mathcal{L}_{2_{x_1}} = 2c_3 q q' \{ (\beta + 1'x_1)[(\beta x_1 + 1) f_1 - \beta x_1]$$

$$+ [\beta (f_1 - 1) + (\beta x_1 + 1) f_{1_{x_1}}] \} \tag{46}$$

$$\mathcal{L}_{2_\alpha} = 2c_3 q q' (\beta x_1 + 1) f_{1_\alpha} \tag{47}$$

APPLICATION TO SPACE SHUTTLE TRANSITION

The numerical results presented in this section demonstrate a variety of planar transition trajectories for a delta-winged configuration of the space shuttle orbiter.[8] The vehicle has a maximum hypersonic L/D of 2.1, which occurs at $\alpha = 13.8°$, and a subsonic L/D_{max} of 4.3 ($\alpha = 8.4°$); the wing loading is 49 psf. The nominal starting point for these trajectories occurs at an altitude of 150,000 ft and a velocity of 8,000 fps, corresponding to a specific total energy of 1.15×10^6 ft; the nominal terminal point at 40,000 ft altitude and 870 fps velocity (M = .9) yields a specific total energy of 5.18×10^4 ft. At the beginning of the transition trajectory, kinetic energy makes the larger contribution to total energy, whereas potential energy is the larger contributor at the end point. Flight is nominally horizontal at the start and ends with a flight path angle of -18°, which is representative of the equilibrium angle during the terminal area glide.

These results show the detailed effects of range control, a comparison of the flat-earth trajectories with round-earth paths, and variations due to changes in initial conditions. A convergence example is presented with a discussion of the feasibility of "real-time" optimization. It will be shown that the "jump" to the "front-side of the L/D curve" need not be made until the very end of the transition, that the dynamic model provides a conservative range estimate, and that the present formulation suggests several alternatives for real-time trajectory control.

Trajectories to a Given Range

This section concentrates on the numerical results achieved for five terminal-ranges, which are bounded by the L/D_{max} case at the upper end and by a maximum load factor of 3 "g's" (approximate) at the lower end. Terminal range varies from 250 nmi to 402 nmi for these cases, all of which have the same initial and final specific energy. The 350 nmi case closely approximates the range-open optimum. It will be seen that the phugoid oscillation is not entirely eliminated by the dynamic pressure-rate penalty – a point of diminishing returns was inevitably reached in the iterative process. Because the phugoid is a natural mode of response, it is put to good use matching initial and final conditions. Furthermore, with the exception of the L/D_{max} case, the maximum dynamic pressure peaks never exceed 234 psf, hardly more than the 190 psf of the nominal terminal condition and not a constraining factor for structure or control.

These trajectories are summarized in Fig. 2, which presents the variation of velocity with altitude. The H-V profile is a direct indication of the energy distribution on the transition flight paths. While flight at L/D_{max} is generally considered to provide a smooth dynamic environment, it evidences the largest phugoid oscillations and dynamic overpressures of this section, largely due to the initial flight condition. The initial condition is not matched to an equilibrium glide, and the vehicle falls into a maximum q of 425 psf. A brief pitch-up at the beginning of the transition phase absorbs the oscillation and provides a flight path with a maximum q of 234 psf, losing 7 nmi of range in the process. The 402 nmi range of the L/D_{max} case could not be improved upon in the numerical optimization. Comparison of the five trajectory profiles with the constant-q curves plotted in Fig. 2 illustrates the general result that increasing range corresponds to increasing q, while the intersections with constant-E curves show the corresponding result that

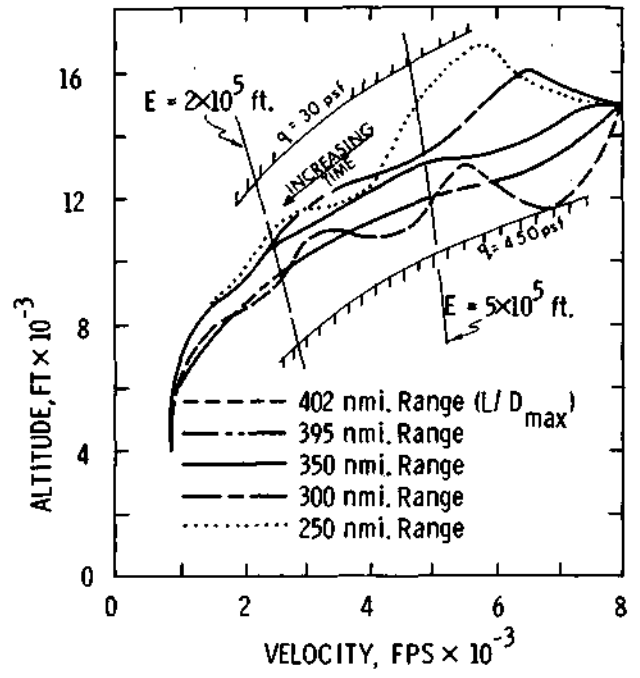

Figure 2. Altitude-velocity profiles for trajectories to several terminal ranges. Initial- and final specific energies are fixed for these 5 cases. Phugoid oscillations cause dynamic pressure peaks. Range increases correspond to higher dynamic pressure.

(ignoring the phugoid mode) long-range trajectories have proportionately higher kinetic energy at a given specific energy level. One sees evidence of the "zoom-climb/zoom-dive" and maximum-E segments which arise from analytic solutions for similar cases,[2] although the effects of finite γ rate-of-change and fixed terminal range cannot be ignored. The H-V trajectories converge to similar profiles near the end point, suggesting that the optimal terminal transition maneuvers are relatively independent of range.

That terminal state and control histories are similar is verified by Fig. 3, 4, 6 and 7. The L/D_{max} case is not constrained to a particular terminal flight condition (other than identical specific energy); hence the terminal velocity is 50 fps lower and the altitude is 1300 ft higher than nominal. The maximum terminal variation from nominal for the remaining four cases is less than 1/6 of these numbers, while the average variation is considerably less.

Figure 3, which presents α and θ as functions of E, illustrates the large initial separation in angles for differing terminal-ranges and the convergence on similar profiles as the end point comes near. Notice in particular that α is virtually always greater than the α required for L/D_{max} (Fig. (3a)) and that abrupt changes in θ (Fig. 3(b)) occur near $E = 10^5$ ft, corresponding to an M of about 1.2 and altitudes of 75,000 - 80,000 ft. The phugoid oscillation is generally apparent in θ but not α; because $\gamma = \theta - \alpha$, it is seen in flight path angle as well. The two shortest range cases require high α at the start of transition to dissipate specific energy and shorten the range. Figure 4(b) shows that maximum load factors are associated with the range adjustment early in the transition, are close to 1 for a large portion of this mission phase, and show an increase associated with the terminal pull-up to the desired flight path angle (γ reaches a minimum of -21.3°).

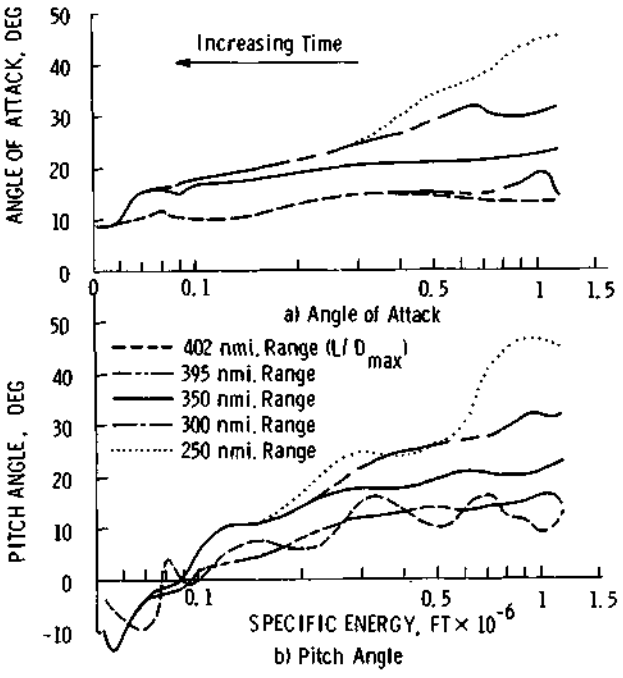

Figure 3. Angle of attack (α) and pitch angle (θ) as functions of the specific energy (E) for several terminal ranges. α remains on the "back side of the L/D curve" for all cases.

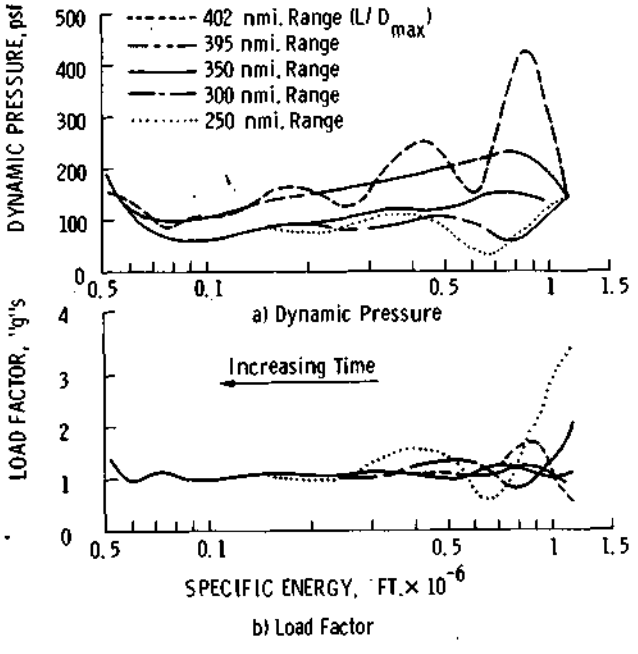

Figure 4. Dynamic pressure (q) and load factor ("g's") as functions of E for several terminal ranges. The greatest q excursions occur for flight at L/D_{max}, due to non-equilibrium starting conditions.

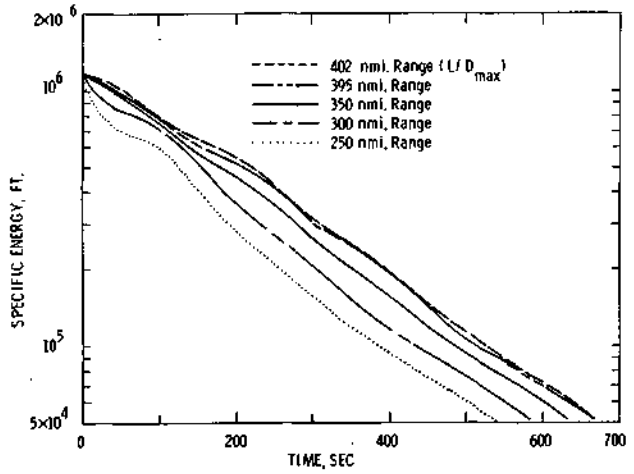

Figure 5. The relationship between the logarithm of specific energy (E) and time is nearly linear, with the slope determined by final range.

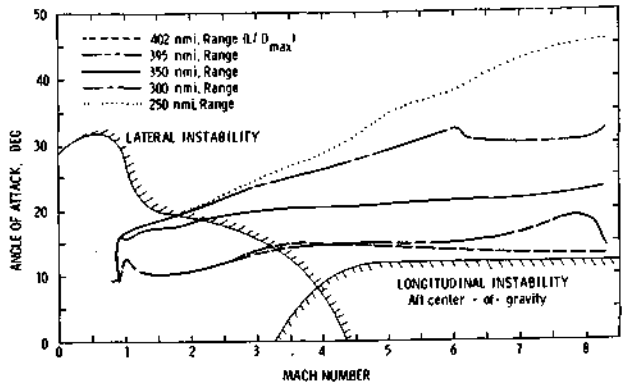

Figure 7. Angle of attack (α) vs. Mach number (M) for several terminal ranges. Stability boundaries are typical.

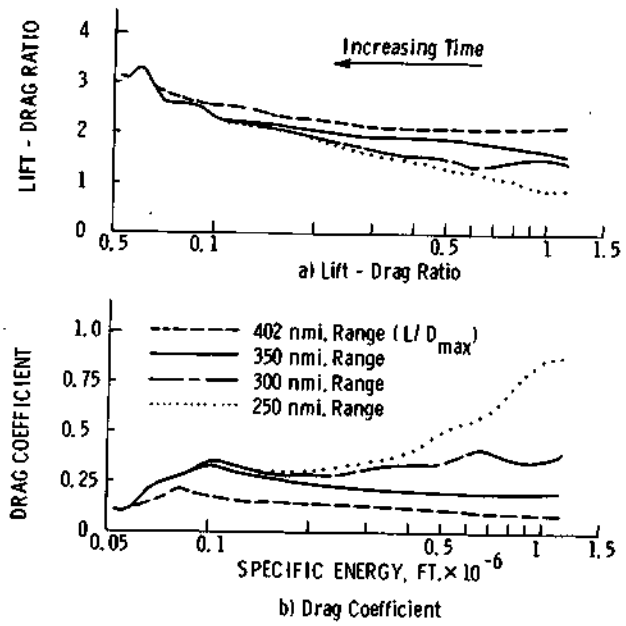

Figure 6. Lift-drag ratio (L/D) and drag coefficient (C_D) as functions of E for several terminal ranges. Drag modulation is seen to be the principal means of range adjustment.

The qualitative relationship between specific energy and time is simple: the logarithm of E decreases nearly linearly with time, and the approximate slope is a function of the final range. Figure 5 illustrates the precise relationship, which contains some oscillation as well as a small mean curvature.

Figure 6 shows that the principal means of adjusting range is in modulation of the drag coefficient (C_D). The lift-drag ratio changes with C_D and is instrumental in maintaining a smooth flight path. To this extent, the shape of the C_D profile is determined by L/D modulation; however, the average magnitude of C_D is a more significant function of desired final range than is L/D.

A plot of α vs. M (Fig. 7) again shows that there is no important requirement for flight on the front side of the L/D curve. Flight at lower α requires higher q, a condition to be avoided if dynamic pressure peaks are a major concern. As shown previously,[1] the final reduction in α to the trim-glide angle occurs at nearly constant, subsonic M. Mach number actually decreases to .85 before taking its final value of .9. The α-M plot finds its greatest use in defining the stability and control environment, as both parameters have strong effects on vehicle aerodynamics. Typical boundaries along which short-period and Dutch roll modes of longitudinal and lateral-directional angular motion[5] become statically unstable are superimposed on Fig. 7. The α-M profiles are shown to avoid longitudinal instability, but flight in a region of lateral-directional instability is unavoidable for M above 2 to 3. Stability augmentation is therefore required for the lateral-directional mode.

Errors Due to the Simplified Dynamic Model

Elimination of the round-earth terms in the equations of motion and the small γ assumption lead to errors in trajectory computation. Ignoring centrifugal force effectively reduces the lift on the vehicle, causing pessimistic estimates of range (too short) and dynamic pressure (too high). Gravitational acceleration is overestimated at the beginning of the trajectory and underestimated at the end; however, the altitude span is not large, and this simplification has small effect. Range is overestimated by neglecting the earth's curvature. The γ assumption leads to an overestimate of gravitational effects on K' and γ', while the range calculation is increased by assuming a horizontal velocity vector.

The over-riding effect is the lack of centrifugal force. A comparison of the simplified calculations with a round-earth model which neglects oblateness and rotational effects shows range

increases of 3% to 5% for ranges of 250 to 402 nmi for the latter, while maximum dynamic pressure is reduced from 0% to 16%. Both errors are conservative, as the actual trajectory is flown with lighter aerodynamic loads, and the terminal-range is reached with excess specific energy. Restoring centrifugal force to the equations would correct the principal error and cause small additional complexity. A pragmatic approach would be to bias the target range.

Initial Condition Effects

Two kinds of initial condition effects are considered: those which are accounted for by recomputation of the optimal control and those which are not. In both cases the control is a function of E; hence, there is feedback of altitude and velocity, and terminal V, γ, and H are close to the desired values. The primary difference is whether or not range is controlled. This difference is reflected in the early control history, and, therefore, in the most significant q peak.

A variation in initial velocity with range controlled to 350 nmi has counter-intuitive effects on load factor and dynamic pressure. Variations of $\pm$500 fps have small effect on maximum load factor, but the result is an increase for both positive and negative variations. The negative variation causes a substantial increase in maximum q, while the positive variation shows reduced q. These results can be attributed to the phase of the phugoid oscillation induced by range control. Lower initial velocity leads to lower E_o, causing the vehicle to fly at lower α to stretch the range. As shown by Fig. 8, the loss of lift causes H to drop and q to rise. The opposite is true when there is excess energy.

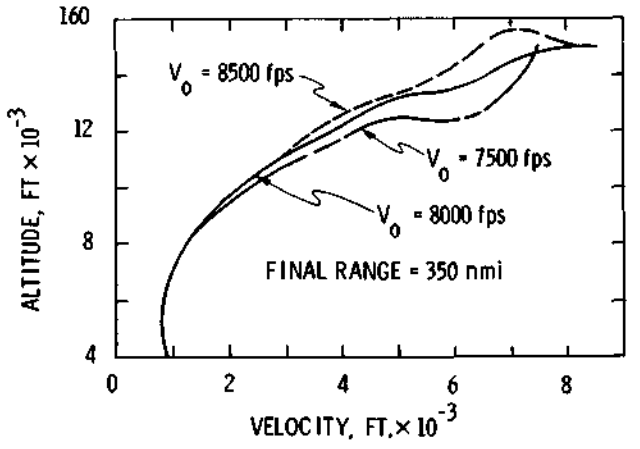

Figure 8. The effect of initial velocity on flight paths to 350 nmi final range. Low initial velocity causes descent to lower altitude, increasing dynamic pressure.

Flight path angle variation (with range controlled) has an equally interesting effect. Raising the initial γ provides ballistic lengthening of the trajectory. Angle of attack increases to shorten the range, and maximum q is reduced.

Results obtained with initial state variations and a single near-optimal α-E profile for 350 nmi final range are summarized in Table I. The effects of the initial variations are computed for the round-earth model. The table shows that final V and γ are virtually insensitive to the initial variations, and H_f sensitivity is small. Scheduling α as a function of E (and thus H and V) provides effective closed-loop control of the terminal altitude and velocity vector. The same cannot be said for final range, which shows small changes with initial altitude variation, moderate change with γ, and large change with V (which, in this case, represents a large change in E_o). The increase in maximum load factor is greatest with the $-\gamma$ variation, and the $+\gamma$ variation provides a 40% increase in maximum q.

Case	V_f, fps	γ_f, deg	H_f, ft	R_f, nmi	q^*_{max}, psf	Load factor	E_o, ft$\times 10^{-6}$
Nominal (Flat-Earth)	868	-18.2	40052	350.1	171	1.47	1.15
Nominal (Round-Earth)	854	-16.5	40458	366.	152	1.46	1.16
+500 fps	854	-16.5	40449	405.6	120	1.44	1.29
-500 fps	854	-16.5	40465	327.9	157	1.48	1.04
+3°	854	-16.5	40464	383.4	211	1.59	1.16
-3°	855	-16.7	40569	348.1	201	1.66	1.16
+5000 ft	853	-16.5	40466	368.7	172	1.36	1.16
-5000 ft	854	-16.5	40468	363.1	182	1.64	1.15

* Excluding end points

Table I. Effects of initial condition variations on a 350 nmi transition trajectory.

Real-Time Applications

The alternatives available for "real-time" optimal trajectory control fall into three categories: on-line solution of the two-point boundary-value problem, linearization about a nominal flight path to obtain optimal feedback gains, and dynamic programming. The present investigation was motivated by the first alternative but could be useful for the remaining two alternatives as well. In any case, a practical guidance scheme must include a cross-ranging capability, which is not studied here.

Solving the two-point boundary value problem, e.g., the trajectory and optimization equations offered in this paper, is a formidable task even with a ground-based general purpose computer; however, the possibility should not be dismissed without study, for the flexibility that this approach offers is extreme. It is reasonable to assume that only one or two full solutions would be required during the flight as a means of improving the nominal flight path and control for a perturbation guidance law. Nevertheless, integrations along the flight path must be fast, and the process must converge reliably within a few iterations.

The program which computed this paper's numerical results was not "streamlined" for use in a flight computer, but it gives some indication of what might be expected in a real-time environment. Using a variable-energy integration step and single-precision arithmetic, about 100 Runge-Kutta steps were used for each state and adjoint integra-

tion. Near-optimal control-step adjustment required the evaluation of three state histories and one adjoint history for each iteration. Fast convergence is dependent on taking a near-optimal control step on each iteration, and the size of the best step is not easily predicted from the previous iteration. There is no question that starting control profiles, control steps, penalty weights, and adjustment rules must be chosen carefully for fast, reliable convergence; however, convergence of the sort illustrated in Table II has been obtained for a number of cases. The starting profile had V, γ, and R errors of 35 fps, 2.7°, and 16 nmi, with q_{max} = 181 psf; after two iterations, the errors were 2 fps, .3°, and .04 nmi, with q_{max} = 157 psf.

Iteration	Velocity cost	γ cost	Range cost	q' cost	Total cost	$<\delta\alpha, \delta\alpha>$	Step size
0	8.8	.4	985.	8.5	1002.	4645.	—
1	8.6	.4	.01	3.64	12.6	239.	42.
2	.02	.004	.0006	3.65	3.69	.6	4.7
3	.004	.007	.0008	3.67	3.68	.08	6.4

Table II. Convergence example for 350 nmi final range. The inner product, $<\delta\alpha, \delta\alpha>$, is a measure of the proximity to an extremal path.

The energy formulation is amenable to neighboring-extremal linearization, which allows optimal feedback gains to be computed for control about a nominal path.[7] The gains for K(E), γ(E), and R(E) are obtained by evaluating a 3×3 matrix Riccati equation. Although the dimension of this equation is not large, there are a large number of coefficients to be evaluated, many of which are more complex than the coefficients of the original nonlinear equations; hence, the "ideal" combination of computing an optimal trajectory onboard followed by calculation of optimal feedback gains appears impractical. Pre-computed gains scheduled against specific energy would be a better solution, especially since α should remain above the α for L/D_{max} during the largest part of the transition.

A family of optimal transition trajectories constitutes an autonomous field of extremals which can be used for nonlinear feedback control. The theory of dynamic programming[10] proves that there is a unique optimal control variable associated with each point in the extremal field, in this case defined by K (or V), γ, R and E; hence, α can be pre-computed as an optimal function of these variables and stored within the flight computer. A table-lookup algorithm then provides the nonlinear feedback control law. The present results suggest that a two-parameter table, in which the guidance command, α_G, is a function only of E and range-to-go ($R_{GO} = R_f - R$), may be sufficient.

Figure 9 illustrates a planar guidance concept in which $\alpha_G(E, R_{GO})$ is supplemented by dynamic pressure rate damping to make up for the missing

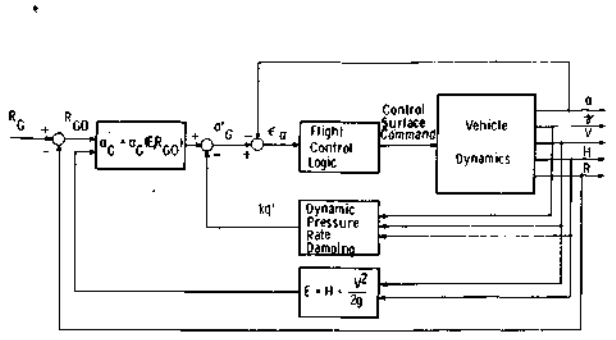

Figure 9. Block diagram of dynamic programming approach to planar guidance (inner loops of flight control system not shown). The guidance command, α_G, is a function of specific energy (E) and range-to-go (R_{GO}).

state variables in the nonlinear function. The dynamic pressure rate can be derived from Eq. (44) and is, therefore, a function of K and γ. The γ-dependence can be eliminated by using Eq. (7) and (13b) instead of Eq. (28) to find f_1, introducing a requirement to measure $\dot{V}$.

Figure 10 illustrates (in perspective) the guidance function, $\alpha_G(E, R_{GO})$, which is derived from the optimal trajectories presented in Fig. 2 to 7. Choosing α to lie on the guidance surface results

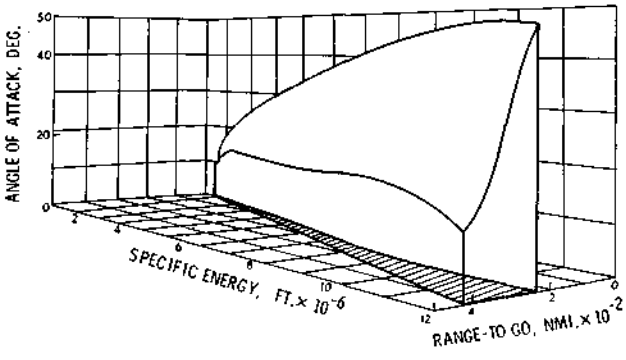

Figure 10. Guidance function, $\alpha_G(E, R_{GO})$, for the planar case.

in a near-optimal trajectory to the end-point, one which yields the desired V, γ, H, and R at the beginning of terminal area maneuvering, while minimizing dynamic pressure rate-of-change. The "shadow" of the surface converges as the final range is approached. Ranging control is effectively terminated in this example several nmi from the end point; the surface becomes a line independent of R_{GO} in order to provide a good match to the desired V_f, γ_f, and H_f.

Table III presents some results of applying the guidance function of Fig. 10 with several initial

Initial Conditions	$V_{f'}$ fps	$\gamma_{f'}$ deg	$H_{f'}$ ft	$R_{f'}$ nmi	q^*_{max} psf	Load factor
Nominal	846	-15.9	40627	350.0	135	1.32
+500 fps	847	-16.0	40645	350.0	115	1.43
-500 fps	845	-16.3	40671	349.9	180	1.62
+3°	846	-16.0	40660	350.0	127	1.31
-3°	846	-15.9	40653	350.0	188	1.46
+5000 ft	846	-16.0	40658	350.0	138	1.32
-5000 ft	847	-16.0	40652	350.0	134	1.31

*Excluding end points

Table III. Trajectories to 350 nmi final range using dynamic programming guidance function.

conditions. No trajectory damping is used on these round-earth paths to a 350-nmi final range. End-point convergence is seen to be very good, and dynamic pressure- and load factor peaks (which could be reduced with trajectory damping) are not excessive.

CONCLUSIONS

The planar gliding path of a space shuttle orbiter (or other aircraft) has been shown to be readily described as a function of specific energy rather than time. Transforming the independent variable reduces the order of the trajectory problem, and introducing kinetic energy as a state variable yields further simplification. The change of variables provides a fixed end-point for the transition trajectory without restricting the final time, a decided asset for flight path optimization. As presented, the equations also are applicable to terminal area maneuvering and landing approach (although only the space shuttle's transition phase has been investigated); the equations could be extended to hypersonic entry with little difficulty.

Trajectory optimization by the steepest-descent method has provided typical results for a delta-wing orbiter configuration. The problem of phugoid oscillation has been reduced by defining a trajectory damping integral penalty function which is quadratic in the rate-of-change of dynamic pressure. The trajectories are shown to occur almost entirely on the "back side of the L/D curve," avoiding the high dynamic pressures associated with low C_L.

The choice of specific energy as independent variable is particularly fortunate for trajectory control, in that optimal control profiles establish a nonlinear feedback relationship from altitude and velocity to angle of attack. A family of optimal trajectories forms a field of extremals suitable for control via dynamic programming. The number of profiles which are necessary for real-time solution is small, because α is a strong function of only two variables. Extending the real-time control to 3-dimensional trajectories introduces a new control variable (roll angle) and a new guidance parameter (crossrange-to-go, or its equivalent). The specific energy formulation and the dynamic programming guidance function are expected to yield advantages for this problem as well.

References

1. Stengel, R. F., "Strategies for Control of the Space Shuttle Transition," AIAA Paper No. 71-921, New York, August, 1971.

2. Hoffman, W. C., Zvara, J., Bryson, A. E., Jr., "A Landing Approach Guidance Scheme for Unpowered Lifting Vehicles," AIAA Journal of Spacecraft and Rockets, Vol. 7, No. 2, Feb. 1970, pp. 196-202.

3. Speyer, J. L., Womble, M. E., Jr., "Approximate Optimal Re-Entry Trajectories," AIAA Paper No. 71-919, New York, August, 1971.

4. Kelley, H. J. "Aircraft Maneuver Optimization by Reduced-Order Approximation," in Advances in Control Systems, Vol. 9, (C. T. Leondes, ed.), Academic Press, New York, 1972.

5. Etkin, B., Dynamics of Atmospheric Flight, John Wiley & Sons, New York, 1972.

6. Zeldin, S., Speyer, J. L., "Maximum Noise Abatement Trajectories," AIAA Paper No. 72-665, New York, June 1972.

7. Bryson, A. E., Jr., Ho, Y., Applied Optimal Control, Blaisdell, Waltham, 1969.

8. Click, P. L., Michna, D. J., Sarver, D. A., "Aerodynamic Stability and Control Characteristics of the NASA/MSC .006 Scale 040-A Delta Wing Orbiter," NASA CR-120015, Huntsville, November 1971.

9. Bryson, A. E., Jr., Desai, M. N., Hoffman, W. C., "Energy-State Approximation in Performance Optimization of Supersonic Aircraft", AIAA Journal of Aircraft, Vol. 6, No. 6, Nov. - Dec. 1969, pp 481-488.

10. Bellman, R., Kalaba, R., "Dynamic Programming and Adaptive Processes," IRE Transactions on Automatic Control, Vol. AC-5, No. 1, Jan., 1960, pp. 5-10.

E-2708

DISTRIBUTION LIST

Internal:

R. Battin
H. Blair-Smith
T. Brand
A. Cook
R. Cushing
J. Deyst
A. Engel
G. Edmonds
P. Felleman
T. Fitzgibbon
J Gilmore
F. Glick
D. Gustafson
E.J. Hall
M. Hamilton
J. Harper
D. Hoag
L. Johnson
M. Johnston
J. Kernan
A. Klumpp
G. Kossuth
B. Kriegsman
J. Laning
G. Levine
T. Edelbaum
A. Hopkins
P. Mimno
E. Muller
J. Nevins
J. O'Connor
E. Olsson
G. Ogletree
R. Ragan
W. Robertson
N. Sears
G. Silver
R. Stengel (10)
G. Stubbs
R. Weatherbee
Apollo Library (2)
CSDL Library (10)
SSV Central Files (4)
D. Fraser
D. Gustafson
Group 23C (25)

External:

NASA/RASPO (1)

Delco (3)

Kollsman (2)

Raytheon (2)

MSC:

National Aeronautics and Space Administration (32 & 1R)
Manned Spacecraft Center
Houston, Texas 77058

Attn: Apollo Document Control Group
(BM 86) (18 & 1R)
R. Chilton
K. Cox (3)
W. Peters (3)
J. Hanaway
F. Elam
G. Zacharias
W. Bradford
S. Mann
J. Williams
T. Price

KSC:

National Aeronautics and Space Administration (1R)
J.F. Kennedy Space Center
J.F. Kennedy Space Center, Florida 32899

Attn: Technical Document Control Office